DEVCOM DAC-TR-2022-094
September 2022

Analysis of Reclined Posture ATD and PMHS Pelvis–Lumbar Spine Component Tests under Vertical Impact

by Narayan Yoganandan, Jason Moore, John Humm, Jamie Baisden,
Frank A. Pintar, Michael Wassick, David Barnes, and Kathryn Loftis

DISCLAIMER

The findings in this report are not to be construed as an official Department of the Army position unless so specified by other official documentation.

WARNING

Information and data contained in this document are based on the input available at the time of preparation.

TRADE NAMES

The use of trade names in this report does not constitute an official endorsement or approval of the use of such commercial hardware or software. The report may not be cited for purposes of advertisement.

DEVCOM DAC-TR-2022-094
September 2022

Analysis of Reclined Posture ATD and PMHS Pelvis–Lumbar Spine Component Tests under Vertical Impact

by Narayan Yoganandan, Jason Moore, John Humm, Jamie Baisden, and Frank A. Pintar

Medical College of Wisconsin

Michael Wassick

Altus Engineering

David Barnes

SURVICE Engineering Co.

Kathryn Loftis

DEVCOM Analysis Center

REPORT DOCUMENTATION PAGE

Form Approved
OMB No. 0704-0188

1. REPORT DATE	2. REPORT TYPE	3. DATES COVERED (From - To)
September 2022	Technical Report	October 2019–August 2022

4. TITLE AND SUBTITLE
Analysis of Reclined Posture ATD and PMHS Pelvis–Lumbar Spine Component Tests under Vertical Impact

5a. CONTRACT NUMBER

5b. GRANT NUMBER

5c. PROGRAM ELEMENT NUMBER

6. AUTHOR(S)
Narayan Yoganandan, Jason Moore, John Humm, Jamie Baisden, Frank A. Pintar, Michael Wassick, David Barnes, and Kathryn Loftis

5d. PROJECT NUMBER

5e. TASK NUMBER

5f. WORK UNIT NUMBER

7. PERFORMING ORGANIZATION NAME(S) AND ADDRESS(ES)
Director
DEVCOM Analysis Center
6896 Mauchly Street
Aberdeen Proving Ground, MD 21005-5071

8. PERFORMING ORGANIZATION REPORT NUMBER
DEVCOM DAC-TR-2022-094

9. SPONSORING / MONITORING AGENCY NAME(S) AND ADDRESS(ES)

10. SPONSOR/MONITOR'S ACRONYM(S)

11. SPONSOR/MONITOR'S REPORT NUMBER(S)

12. DISTRIBUTION / AVAILABILITY STATEMENT
DISTRIBUTION STATEMENT A. Approved for public release: distribution unlimited.

13. SUPPLEMENTARY NOTES

14. ABSTRACT
The experimental design and protocols used in the study showed the feasibility of conducting anthropomorphic test device (ATD) and postmortem human surrogate (PMHS) tests in reclined postures. The tested Generation (Gen)-I version of the Warrior Injury Assessment Manikin (WIAMan) ATD appears to be suitable to evaluate the performance in under-body blast loading under different postures: nominal to recline, potentially reflecting future seat and vehicle designs in the military. The biomechanical responses analyzed from the PMHS data showed that injuries parallel nominal postures and spinal loads can be determined. Mechanical responses from the ATD data demonstrated that component-based contributions of axial and shear forces and bending moments depend on the postural angulation. In this analysis study, the shear factor was used as a biomechanical metric for quantifying the responses of the pelvis–lumbar spine of the Gen-1 ATD because it accommodated both the axial and shear forces in the time domain. Recognizing that the shear factor did not significantly change with different reclined postures considered in this test series, the current injury assessment reference curves developed for the nominal posture may also be applicable to reclined postures with this ATD.

15. SUBJECT TERMS
Warrior Injury Assessment Manikin, WIAMan, lumbo–pelvis, recline, alternative posture, Postmortem Human Surrogate, PMHS, Anthropomorphic Test Device, ATD, pelvis fracture

16. SECURITY CLASSIFICATION OF:			17. LIMITATION OF ABSTRACT	18. NUMBER OF PAGES	19a. NAME OF RESPONSIBLE PERSON
a. REPORT	b. ABSTRACT	c. THIS PAGE			Kathryn Loftis
UNCLASSIFIED	UNCLASSIFIED	UNCLASSIFIED	UU	47	19b. TELEPHONE NUMBER (include area code) (410) 306-0344

Table of Contents

List of Figures

List of Figures

List of Tables

Executive Summary

Introduction

The Warrior Injury Assessment Manikin (WIAMan) anthropomorphic test device (ATD) was developed based on the nominal seated Soldier posture and vertical impact loading with matched-pair postmortem human surrogate (PMHS) tests. Loads at the inferior and superior ends of the lumbar spine and accelerations at the sacrum were used in the ATD injury assessment reference curves (IARCs). While initial testing and IARC developments were based on the nominal posture, new vehicles may include reclined seats. This may alter the interrelationships and intrinsic load paths between the pelvis and spine, and the relative contributions of different biomechanical metrics (e.g., axial force to shear force ratio), injury mechanisms, and IARCs. The extent of the applicability of the current IARCs, developed for the nominal posture, to the reclined posture was not investigated in initial studies conducted by the WIAMan program. The Medical College of Wisconsin (MCW) conducted WIAMan ATD and PMHS tests with selected reclined postures as part of the WIAMan program; however, data were not yet analyzed.

Objectives

The objectives of this study were to analyze previously conducted reclined postural tests with the WIAMan ATD and PMHS pelvis–lumbar spine complexes to understand the feasibility of positioning in reclined postures and compare recline posture results to nominal posture results. ATD tests are described first, followed by PMHS tests.

Analysis of ATD Tests

ATD Methods: The ATD pelvis–lumbar component was positioned on the custom vertical accelerator device in the nominal posture and reclined postures of 17°, 30° and 45°. Impact loading was applied at different velocities. Axial and shear forces and bending moments in the sagittal plane were gathered using the ischial, lumbar, and T12 load cells. Peak axial, shear and resultant forces and moments, and shear forces at the time of occurrence of the peak axial forces were obtained. Shear factor was defined as the ratio of the shear force at the time of peak axial force to the peak axial force and this metric was compared for the nominal and reclined test series. The factor was also compared using the resultant force.

ATD Results: Data from 53 tests were analyzed: 20 in the nominal, 14 each in the 17° and 45°, and 5 in the 30° reclined postures. The seat plate velocities for all postures ranged from 1.7 to 7.4 m/s. Axial and shear forces and bending moment data are provided in the body of the report. Shear factors for the 0°, 17°, 30°, and 45° reclined

posture tests at the T12 location were 0.47 ± 0.09, 0.26 ± 0.04, 0.09 ± 0.06, and 0.07 ± 0.05, respectively. At the lumbar location, they were 0.07 ± 0.05, 0.02 ± 0.02, 0.04 ± 0.02, and 0.09 ± 0.03, respectively. Appendix A includes the test matrix and regression plots of the forces versus velocities for each posture. Time histories of the three forces (axial, shear, and resultant) and bending moments at the three locations, and shear factors are provided in a separate summary report.

ATD Summary: Reclined postures were expected to involve differing proportions of axial and shear forces at the T12 and lumbar locations on the spine. Using this as a basis, the shear factor metric was defined to include the temporal development of both force components, addressing potential injury mechanisms. Shear factors at the T12 location were 0.5 for the nominal, 0.3 for the 17° recline, and 0.1 for the 30° and 45° recline postures. The same trend in the shear factor was found when the axial force was replaced by the resultant force, while the magnitudes were lower in all cases. Shear factors were lower for the lumbar location in both cases. Analysis from other tests in the WIAMan database can be included to reinforce the present findings. Analysis of PMHS tests is summarized as follows.

Analysis of PMHS Tests

Methods: Two PMHS pelvis–lumbar spines component specimens were procured according to the WIAMan criteria and pretest X-ray, and computed tomography (CT) images were obtained. The contents of the pelvic cavity were removed while maintaining the integrity of the skin and associated tissues. The specimens were embedded in polymethylmethacrylate at the L4 vertebra level, and a six-axis load cell was attached to the superior end of the fixation. Appropriate weights were added to represent the mass of the pelvic and surrounding abdominal contents and effective mass of the torso to the respective regions of the specimen. Uniaxial accelerometers and strain gages were placed on the pelvis and spine, and accelerometers and load cells were placed on the seat platen of the custom vertical accelerator device to measure forces, strains, and accelerations.

The specimens were placed on a custom vertical accelerator device. Corresponding to the 45° recline angle of the WIAMan ATD test, the angle of the pelvis was 58° in the first specimen (termed as PV0200) and 61° in the second specimen (termed as PV0201). Pretest X-rays were obtained while the specimen was on the platform of the accelerator device. X-rays and CT scans were taken after the test and dissection was performed. Imaging data were used to identify injuries by a neuro-spine surgeon. Axial and shear forces and bending moments in the sagittal plane were gathered at the superior end of the specimen using a six-axis load cell. Axial force data from the load cell were mass compensated, representing the transmitted loads to the specimen at the spinal end.

Peak axial, shear, and resultant forces, and peak bending moments were obtained. Injuries are described and their scores using the Abbreviated Injury Scale (AIS 2015 version) by two coders (a clinician and a certified coder, authors of this report) are reported.

PMHS Results: The mean age, height, weight, and body mass index, were 61 ± 2.1 years and 167 ± 4.0 cm, 81.4 ± 26.4 kg, and 29.1 ± 7.6 kg/m^2, respectively. For PV0200 and PV0201 specimens, the impact velocities were 8.8 and 10 m/s, respectively. Peak axial and shear forces and moment data measured at the superior load cell (mounted at L4 for both tests) for PV0200 were 2446 N, 9294 N, and 327 Nm, respectively, and for PV0201, these data were 457 N, 11650 N, and 503 Nm, respectively. Injuries to PV0200 included anterior inferior tip fracture of the L4 vertebral body and sacral fractures. Both injuries were considered stable: AIS = 2 each. Injuries to PV0201 included sacrococcygeal fracture-dislocation and facet fracture, bilateral diastasis of the sacroiliac joint, and anterior and posterior pubic rami fractures. Sacroiliac joint and pelvic injuries were unstable (AIS = 4), and the spine injury (AIS = 2) was stable. In a separate Summary Report, time history plots are provided from accelerometers and strain gages at local locations on the spine and pelvis, seat forces, and spinal loads (peak forces and moments).

PMHS Summary: Injuries documented in these two specimens with reclined postures are similar to those reported in previous nominal postural vertical loading experiments conducted for the WIAMan program. The stable moderate type of injury pattern in the PV0200 specimen, and unstable more-severe type of pelvic injury in the second PV0201 specimen appear to be reflective of the greater velocity/energy input.

Summary from Both Surrogate Tests and Recommendations

The experimental design and protocols used in the study showed the feasibility of conducting ATD and PMHS tests in reclined postures. The tested Generation (Gen)-I version of the WIAMan ATD appears to be suitable to evaluate the performance in under-body blast loading under different postures: nominal to recline, potentially reflecting future seat and vehicle designs in the military. The biomechanical responses analyzed from the PMHS data showed that injuries parallel nominal postures and spinal loads can be determined. Mechanical responses from the ATD data demonstrated that component-based contributions of axial and shear forces and bending moments depend on the postural angulation. In this analysis study, the shear factor was used as a biomechanical metric for quantifying the responses of the pelvis–lumbar spine of the Gen-1 ATD because it accommodated both the axial and shear forces in the time domain. Recognizing that the shear factor did not significantly change with different reclined postures considered in this test series, the current IARCs developed for the

nominal posture may also be applicable to reclined postures with this ATD. As reclined postures may be common in future seat designs, and as the WIAMan ATD has already shown its feasibility to be aligned with different postural conditions, the current set of limited PMHS tests and ATD tests provides confidence in additional matched-pair studies. Once injuries, injury mechanisms, and human injury probability curves from PMHSs and IARCs from WIAMan ATD are developed, it is possible to fully quantitate the efficacy of current IARCs-based nominal posture to reclined postures.

1. INTRODUCTION

The Medical College of Wisconsin (MCW) completed a series of pelvis–lumbar spine tests with the nominal posture using the Warrior Injury Assessment Manikin (WIAMan) anthropomorphic test device (ATD) that paralleled matched-pair tests with postmortem human subjects (PMHS).[1] The nominal posture was defined based on the pelvis and lumbar spine orientation results from a previous seated-Soldier study.[2] Loads at the inferior and superior ends of the spine and sacrum accelerations were used as injury metrics for developing injury assessment reference curves (IARCs) for the WIAMan ATD.

The reclined seating option is an upcoming potential design feature in military vehicles. The posture of the Soldier in reclined seats differs from the nominal posture. This may alter the interrelationships and intrinsic load paths between the pelvis and spine, and the relative contributions of different biomechanical metrics (e.g., axial force to shear force ratio), injury mechanisms, and IARCs. Occupant orientations such as lumbar curvature may also influence posture. The extent of the applicability of the current IARCs developed for the nominal posture to the reclined posture was not investigated in initial studies conducted by the WIAMan program. The analysis of those data is the focus of this report with the recognition that posture alters the internal load paths and biomechanical metrics, while under certain magnitudes of reclined posture angulations, current nominal posture IARCs may be applicable.

With the objectives mentioned, and following the initial studies with the nominal posture, MCW previously conducted WIAMan ATD and a limited number of PMHS tests with selected reclined postures to determine the injuries and biomechanics of the pelvis–lumbar spine with the PMHS and mechanical responses with the ATD pelvis–spine component models. The intent was to determine the feasibility of positioning the ATD in off-nominal postures and conduct tests simulating under-body blast loading in the same vertical accelerator device used for the nominal posture. The intent of the PMHS tests was to demonstrate the feasibility of tests in the reclined posture and compare injuries with results from nominal posture tests. While earlier tests showed the feasibility of both surrogate models to position in off-nominal orientations and respond to vertical loading from the seat to the pelvis, data from both ATD and PMHS surrogates were not analyzed from reclined tests.[3]

2. OBJECTIVE

The objective of this report is to analyze the recently conducted ATD and PMHS tests. Specifically, the analysis focused on mechanical responses of the pelvis–lumbar spine component of the WIAMan ATD in expected reclined postures, and on the injury biomechanics of the PMHS pelvis–spine complex. ATD studies are described in the first part of this report, followed by PMHS in the second part of the report.

3. METHODS

3.1. WIAMan ATD Component Preparation, Mounting, and Instrumentation

The ATD pelvis, pelvis skin, and lumbar spine components were affixed per normal configuration, and the abdominal insert was not included. The pelvis–lumbar spine assembly was mounted at the top of the spine, via a 12-kg ballast mass, to a carriage that translated vertically along a stanchion of the custom vertical accelerator device used for the nominal posture tests.[4] The mount included a wedge that aligned the global x-z coordinates with a six-axis load cell (Model M3944, Sunrise Instruments) on the spine and crosshairs on the pelvic skin. The ATD pelvis was positioned on the seat. The seat was segmented with five plates, five uniaxial load cells (anterior left and right: Interface LWPF1-20kN and posterior left, right, and middle: Interface LWPF1-50kN) were attached to each segment, and all segments were attached to a single platen. Uniaxial accelerometers were attached below the seat platen to each seat load cell and velocity profiles were obtained from the seat platen accelerometer data. Uniaxial accelerometers attached superior to the thoracic end of the spine were used for mass compensation. The pelvis–lumbar spine assembly was aligned such that its sacral load cell was directly superior to the center of the middle of the posterior seat load cell. The pelvis–lumbar spine along with its load cells at the superior and inferior ends were attached to the custom vertical accelerator device that consisted of two components.[4] The standard WIAMan ATD pelvis and lumbar sensors, that is, public rami load cells, ischial tuberosity load cells, sacrum load cell, pelvis 6DX, and lumbar load cell were included in these tests, while the ATD T12 load cell and 6DX were not included. A higher capacity six-axis load cell (Model M3944, Sunrise Instruments) was attached between the superior lumbar spine and mounting block. Given the proximity of this load cell to the superior lumbar spine of the ATD, it is referred to as “T12” in this report.

3.2. Testing Device and Loading

Figure 1 shows the vertical accelerator device. The impact component consisted of a stanchion fixed to the laboratory wall, a cart assembly, and a V-shaped lever arm attached to the seat platen. The drop-cart assembly allowed vertical motion along the stanchion and weight adjustments. The cart mass was released with a predetermined height and impacted the lever arm, accelerating the specimen off the seat platen and up the free-standing impact-receiving component. This component allowed positioning on the seat platen and mounting of the superior end of the ATD to a cart and vertical track that constrained the preparation to postimpact vertical translation. An inspection was performed with rubber skin removed prior to and intermittently throughout the testing

sequence. The integrity of the internal pelvic components, lumbar lamination, and skin (rubber) abrasion at the impact site were examined during the testing process.

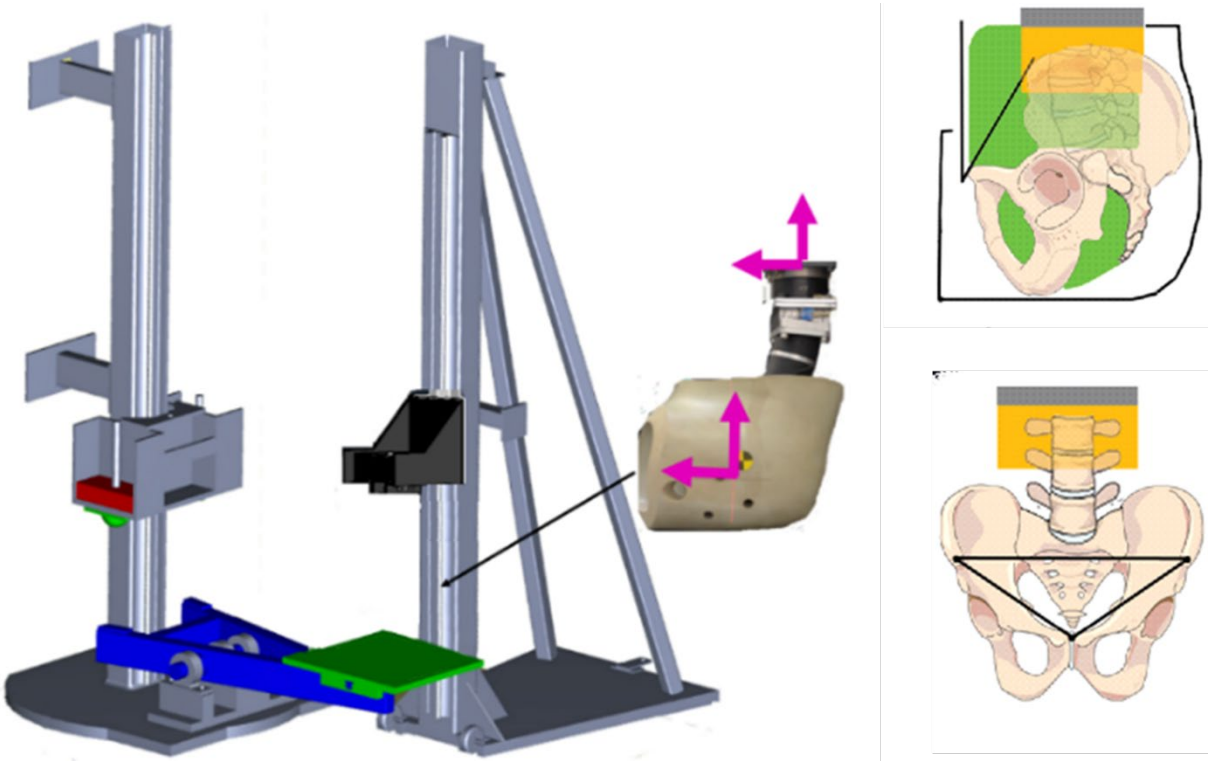

Figure 1. Schematic of the vertical accelerator with the photograph of the two components and WIAMan ATD. Arrows point to the x (right-to-left) and z (inferior-to-superior) axes. The load cell is shown on the top of the lumbar spine of the ATD. The two schematics of the human pelvis–lumbar spine on the right shows the load cell as a shaded gray rectangle on top of the orange rectangle illustrating the added mass, and the green-shaded area shows the added surrounding abdominal mass.

Three reclined postures were defined based on the orientation of the lumbar spine at 17°, 30°, and 45°, while the posture included three settings: seat pan, pelvis, and lumbar spine angles.[3] These reclined postures are associated with seat back angles of 15°, 30° and 45° degrees, respectively. The seat pan angle was set with wedges beneath the seat pan, the pelvis angle was set by the external crosshairs on the pelvic skin, and the lumbar spine angle was set by an adjustable mounting plate on the top of the spine attached to the carriage of the vertical accelerator device, shown in Figure 1. The seat back was not included in the study. The angles of the lumbar spine, seat pan, and pelvis associated with the three simulated reclined seat back angles are shown in Table 1. Figures 2 and 3 show the ATD aligned in the nominal and representative reclined postures. In Figure 2, the lateral views of the ATD with and without pelvis flesh show the placement of the skeleton ATD (without flesh) to indicate the load path. The anterior view of the ATD without flesh also illustrates the load path via the bilateral ischial load cell. All tests were conducted in all postures including the nominal posture

tests with intact pelvis, while the denuded flesh was meant to demonstrate the main load-bearing features/paths of the WIAMan ATD. Figure 4 shows a similar diagram for the test setup with the reclined posture.

Table 1. Angulations of the Different Components for Different Postures

Component	Nominal Posture	Reclined Posture (deg)		
	0	17	30	45
Simulated Seat Back	0	15	30	45
T12	0	17	30	45
Seat Pan	0	5	10	15
Pelvis Rotation	0	9	14	18

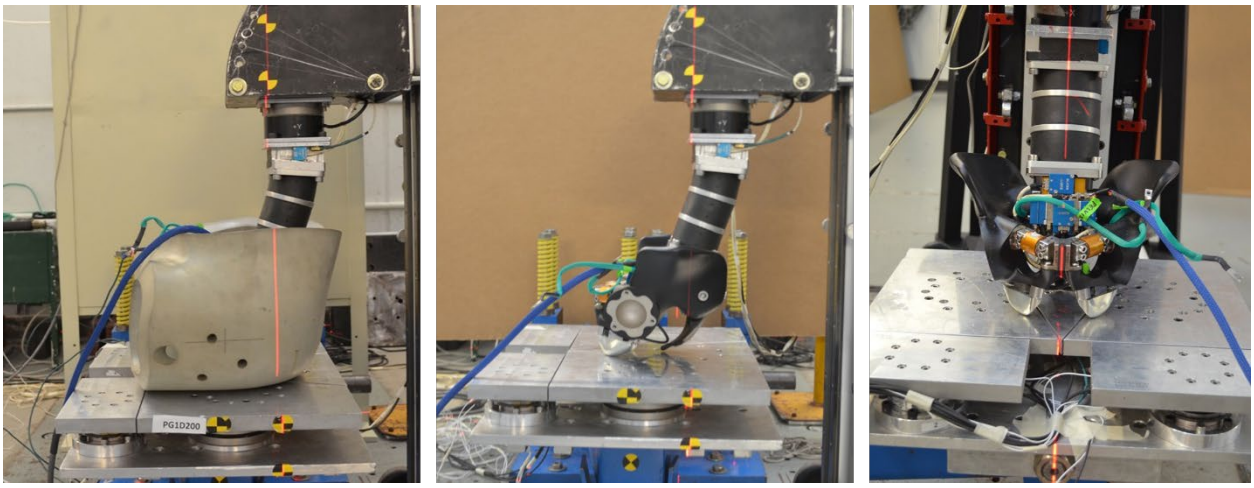

Figure 2. ATD aligned in the nominal posture. Left two photos show the lateral views with and without pelvis flesh. The photo on the right shows the frontal view of the ATD without flesh. The seat platen and seat load cells are also seen.

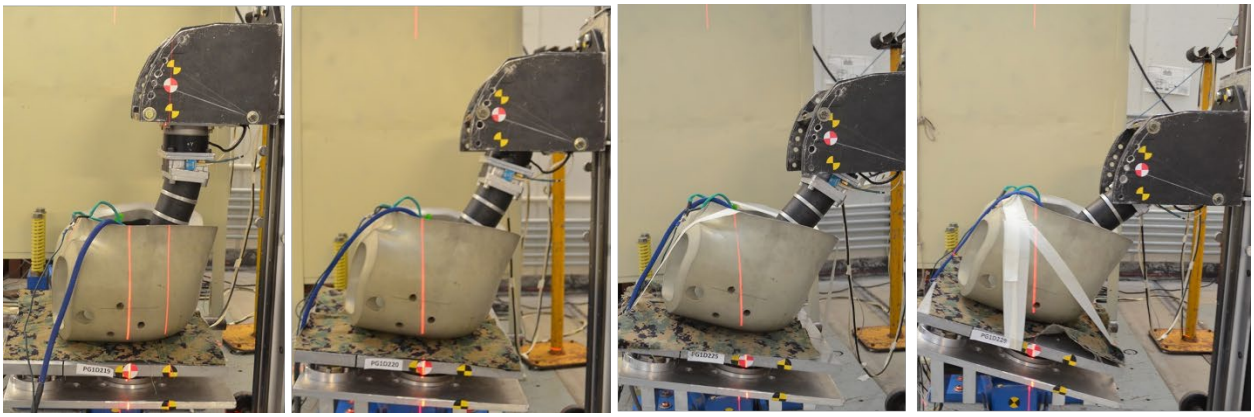

Figure 3. ATD aligned in the reclined posture. Left two photos show the lateral views with and without pelvis flesh. The two photos on the right show the frontal views of the ATD. The seat platen and seat load cells are also seen.

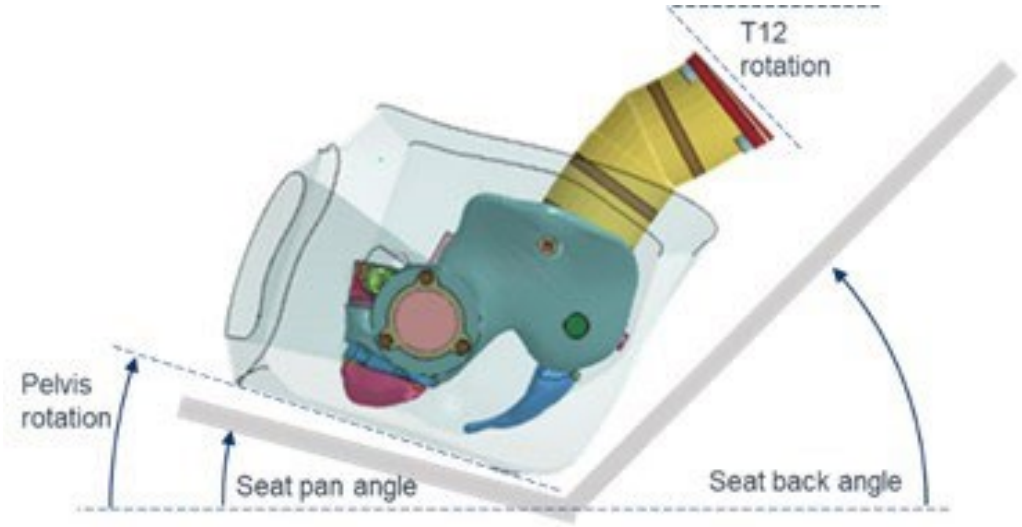

Figure 4. Definitions of the angulations of different components for the reclined posture tests. T12 rotations of 17°, 30°, and 45° were used as the nomenclature for the three reclined angles (Table 1).

3.3. Data Acquisition and Analysis

Sensor data were acquired at a sampling rate of 100 kHz. Force and acceleration signals were processed using a four-pole Butterworth low-pass filter at class 1000. Axial and shear forces in the sagittal plane and resultant force time histories were obtained: axial forces represented the force along the length of the spine, and shear forces represented the force orthogonal to the axial force. In other words, forces were not aligned along the global axis; instead, they represented the axial compressive or tensile and antero-posterior or postero-anterior shear force components sustained by the lumbar spine at the two ends. This was also applicable for the ischial load cell data. Forces and moments (Table 2) were obtained. During the loading phase, maxima compressive axial and shear forces and moments (regardless of direction) and peak resultant forces were obtained for all tests and they were grouped based on the recline angle. The ratio of the shear force at the time of the peak of the axial force during loading event, termed as the shear factor, and the time histories were obtained.

Table 2. Metric Description

Metric	Description
Peak $-F_z$	Peak compressive axial force
Peak F_x	Peak shear force along antero-posterior ($+F_x$) or postero-anterior direction ($-F_x$)
Peak M_y	Peak bending moment in the sagittal plane, flexion ($+M_y$) or extension ($-M_y$)
Peak F_r	Peak resultant force calculated from the F_x and F_z signals
F_x/F_z Shear Factor	Shear force measured at the time of peak compressive axial force
F_x/F_r Shear Factor	Shear force measured at the time of peak resultant force

3.4. PMHS Preparation, Mounting, and Instrumentation

The protocol for human cadaver research was approved by the local institutional board and U.S. Army Human Research Protection Office. The experimental design consisted of isolating the lumbar–pelvis from L4 to acetabulum with musculature and abdominal skin, while removing the femora. PMHSs were screened to ensure there was no presence of blood-borne pathogens or spinal or pelvic abnormalities that may affect biomechanical injury outcomes. Pretest X-rays and computed tomography (CT) scans were obtained. Bone mineral density of the spine was obtained from quantitated CT images. The inclusion–exclusion criteria were such that all subjects were male, there were no previous surgical interventions to the lumbo–pelvis, and there were no bridging osteophytes or congenital fusion of the spine–pelvis complex. The WIAMan inclusion–exclusion criteria were male-only specimens, 18 to 80 years, stature 165 to 186 cm, weight of 64 to 106 kg, and body mass index 18 to 35 kg/m^2.

While preparing the specimen, the contents of the pelvic bowl were removed; however, the ligamentous structures along the lumbar spinal column and within the pelvic ring were maintained intact. The specimen was embedded in polymethylmethacrylate at L4. A 2.7-kg mass and an 8.5-kg mass were added to represent the mass of the pelvic and surrounding abdominal contents. The 2.7-kg mass was within the pelvic cavity, contouring the pelvic bowl from the rami inferiorly to the distal sacrum. The abdominal mass of 8.5 kg was a cylindrical mold set atop the previous gel setting, surrounding the ilia and lumbar segments.[1] The specimen was mounted at L4, via a 12-kg ballast mass to account for the effective mass of the torso (Figure 5, mass shown in gray rectangle; Table 3 lists the accelerometers and strain gages), to a carriage that translated vertically along a stanchion of the custom vertical accelerator device used for the matched-pair nominal posture tests.[1,5] The specimen was positioned on the seat. The seat was segmented with five plates, five uniaxial load cells were attached to each segment, and all segments were attached to a single platen. Uniaxial accelerometers were attached below the seat platen to each seat load cell and velocity profiles were obtained. A six-axis load cell (Denton 3300 J; Humanetics Innovative Solutions) was attached to the superior end of the fixation embedded in the L3 vertebral body. A uniaxial accelerometer was attached at the superior end of the specimen for mass compensation. Figure 5 shows the approximate locations of the instrumentation. The specimen was aligned such that its sacral load cell was directly superior to the center of the middle of the pelvis. The superior end of the spine was angulated by 45° in both specimens, while the orientation of the pelvic recline was based on the anatomy of each specimen. The preparation was attached to the cart on the impact-receiving component of the custom vertical accelerator.

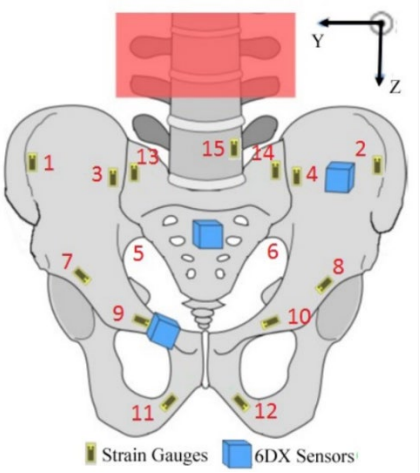

Figure 5. Instrumentation depicted in the schematic of the specimen

Table 3. Summary of Sensors

Location of the Sensor on Figure 5	Sensor Type and Location
1,2	Mid-ilium strain gage
3,4	Ilium near sacroiliac (SI) joint strain gage
5,6	Posterior pubic ring strain gage
7,8	Anterior pubic ring strain gage
9,10	Superior pubic rami strain gage
11,12	Superior pubic strain gage
13,14	Sacrum strain gage
15	L5 body strain gage

3.5. Testing Device, Loading, Imaging, and Injuries

The custom vertical accelerator device used for ATD tests, described earlier (Figure 1), was also used for PMHS tests. The free-standing impact-receiving component of the device allowed positioning the PMHS specimen on the seat platen and mounting the specimen's superior end to its cart. The vertical track constrained the preparation to vertical translation upon impact loading from the level arm and seat platen of the device. The mounting included a six-axis load cell affixed to the specimen potting that constrained the superior end of the preparation. Pretest X-rays were obtained while the specimen was on the platform of the accelerator device and the specimen was subjected to vertical impact at a target velocity of 10 m/s. X-rays and CT scans were taken after the test and the images were used to identify and score the injuries. A practicing neuro-spine surgeon identified the injuries. They were scored using the Abbreviated Injury Scale, AIS 2015 version.[6] One AIS-trained practicing clinician (JLB, an author of this report) and the other a certified AIS coder and biomedical engineer

(KL, also an author of this report) served as two independent observers. Both were blinded to the association of the specimen identity and full testing sequence/details.

3.6. Data Acquisition and Analysis

Sensor data were acquired at a sampling rate of 100 kHz. Force and acceleration signals were processed using a four-pole Butterworth low-pass filter at class 1000. Axial forces from the load cell were mass compensated—representing the transmitted loads to the specimen at spinal end. Axial and shear forces in the sagittal plane and resultant force time histories were plotted for each specimen. Axial forces (F_z, negative, denotes compression) represented the force at L4, and shear forces (F_x, positive, along the antero-posterior axis) represented the force orthogonal to the axial force. In other words, forces were not aligned along the global axis; instead, they represented the axial compressive or tensile and antero-posterior or postero-anterior shear force components. During the loading phase, maxima compressive axial and shear forces and bending moments (M_y, positive, denotes flexion), and peak resultant forces (F_r) were obtained for both specimens.

4. RESULTS

4.1. ATD Test Matrix and Summary of Forces and Force Ratios

A total of 53 WIAMan ATD tests were analyzed: 20 in the nominal, 14 each in the 17° and 45°, and five in the 30° reclined postures. The test matrix is shown in Appendix A. The velocities for all postures ranged from 1.2 to 7.4 m/s. Data including time histories of the axial, shear and resultant forces, and shear factor data for each test is held by the U.S. Army Combat Capabilities Development Command (DEVCOM) Analysis Center, known as DAC, and may be requested.

4.2. ATD Peak Forces and Shear Factors Based on Recline Angles

For the nominal posture, the velocities ranged from 2.5 to 3.7 m/s (mean: 2.7 ± 0.4 m/s). The F_x/F_z shear factor ranged from 0.29 to 0.59 for the T12, from 0.01 to 0.21 for the lumbar, and 0.02 to 0.15 for the ischial regions. Other data are summarized in Table 4.

Table 4. Summary of Peak Axial, Shear and Resultant Forces, and F_x/F_z Shear Factor for the Nominal Posture (Velocity Range: 2.5 to 3.7 m/s)

Value	F_x Peak (N)	F_z Peak (N)	F_r Peak (N)	F_x at F_z Peak (N)	F_x/F_z Shear Factor
			T12		
Min	–3070	–6520	4328	–2984	0.29
Max	–1991	–4175	7142	–1133	0.59
			Lumbar		
Min	–1167	–8228	5166	–1132	0.01
Max	703	–5166	8253	157	0.21
			Ischial		
Min	149	–3322	1257	–108	0.02
Max	373	–1242	3324	263	0.15

For the 17° reclined posture, the velocities ranged from 1.2 to 7.4 m/s (mean: 4.3 ± 1.6 m/s). The F_x/F_z shear factor ranged from 0.17 to 0.33 for the T12, from 0.00 to 0.21 for the lumbar, and 0.12 to 0.25 for the ischial regions. Other data are summarized in Table 5.

Table 5. Summary of Peak Axial, Shear and Resultant Forces, and F_x/F_z Shear Factor for the 17° Reclined Posture (Velocity Range: 1.9 to 7.4 m/s)

Value	F_x Peak (N)	F_z Peak (N)	F_r Peak (N)	F_x at F_z Peak (N)	F_x/F_z Shear Factor
			T12		
Min	–5207	–15820	4214	–5204	0.17
Max	–919	–4152	16654	–718	0.33
			Lumbar		
Min	–1520	–17736	4677	–360	0.00
Max	1309	–4677	17736	301	0.21
			Ischial		
Min	–495	–3666	491	73	0.12
Max	998	–485	3778	908	0.25

For the 30° reclined posture, the velocities ranged from 1.8 to 5.6 m/s (mean: 3.0 ± 1.70 m/s). The F_x/F_z shear factor ranged from 0.02 to 0.17 for the T12, from 0.01 to 0.07 for the lumbar, and 0.11 to 0.35 for the ischial regions. Other data are summarized in Table 6.

Table 6. Summary of Peak Axial, Shear and Resultant Forces and F_x/F_z Shear Factor for the 30° Reclined Posture (Velocity Range: 1.8 to 5.6 m/s)

Value	F_x Peak (N)	F_z Peak (N)	F_r Peak (N)	F_x at F_z Peak (N)	F_x/F_z Shear Factor
			T12		
Min	–2416	–12942	4005	–2249	0.02
Max	–519	–4004	13139	–82	0.17
			Lumbar		
Min	–960	–14913	4236	–736	0.01
Max	488	–4235	14931	73	0.07
			Ischial		
Min	–163	–2474	175	20	0.11
Max	650	162	2509	404	0.35

For the 45° reclined posture, the velocities ranged from 1.7 to 7.4 m/s (mean: 4.3 ± 1.8 m/s). The F_x/F_z shear factor ranged from 0.01 to 0.19 for the T12, from 0.03 to 0.15 for the lumbar, and 0.04 to 0.41 for the ischial regions. Other data are summarized in Table 7.

Table 7. Summary of Peak Axial, Shear and Resultant Forces, and F_x/F_z Shear Factor for the 45° Reclined Posture (Velocity Range: 1.7 to 7.4 m/s)

Value	F_x Peak (N)	F_z Peak (N)	F_r Peak (N)	F_x at F_z Peak (N)	F_x/F_z Shear Factor
			T12		
Min	–3144	–16559	2992	–2534	0.01
Max	1239	–2984	16752	343	0.19
			Lumbar		
Min	–1926	–16525	2952	–1434	0.03
Max	1258	–2946	16547	–181	0.15
			Ischial		
Min	–836	–2938	163	–28	0.04
Max	1040	156	3086	936	0.41

A summary of the mean and standard deviation of the F_x/F_z shear factor data for all postures is given in Table 8. The maximum contribution of the shear force was at T12 (shear factor = 0.47) and the minimum was at the ischial end (shear factor = 0.04) for the nominal posture.

Table 8. Summary of F_x/F_z Shear Factors at All Three Locations and for All Postures

Recline Angle (deg)	No. of tests	Velocity (m/s)		F_x/F_z Shear Factor					
				T12		Lumbar		Ischial	
		Mean	SD	Mean	SD	Mean	SD	Mean	SD
0	20	2.71	0.40	0.47	0.09	0.07	0.05	0.08	0.04
17	14	3.96	1.73	0.26	0.04	0.02	0.02	0.18	0.05
30	5	2.98	1.70	0.09	0.06	0.04	0.02	0.21	0.09
45	14	4.27	1.81	0.07	0.05	0.09	0.03	0.26	0.11

4.3. ATD Variation of Peak Forces Based on Recline Angles

Cross plots of the axial and shear forces at the T12 and lumbar locations for different postures are shown in Figures 6 and 7, respectively. The plots with the same abscissa and ordinate magnitudes demonstrated distinct demarcation at T12; that is, increasing recline angle decreased shear forces, while the pattern was less distinct at the lumbar location.

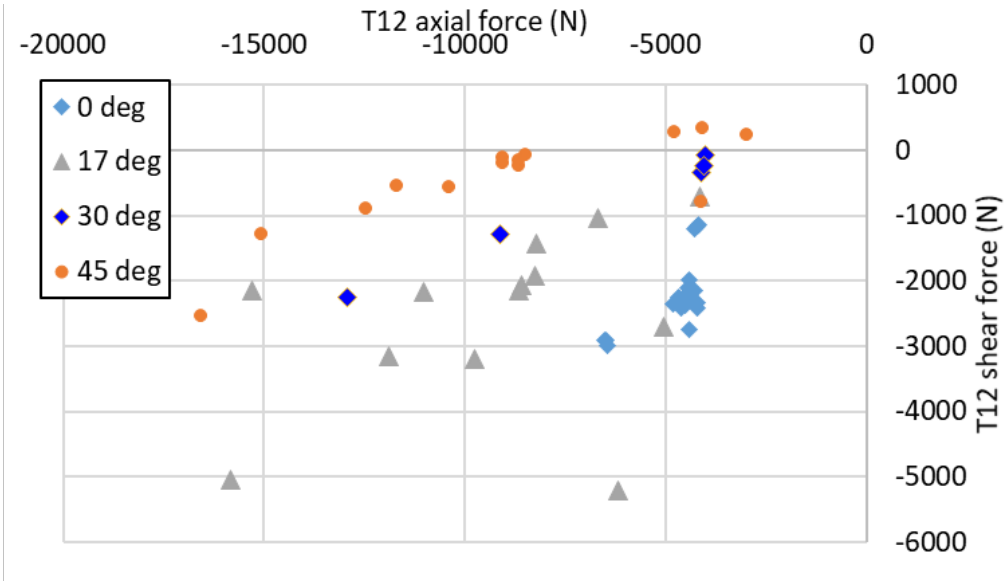

Figure 6. Cross plot of the T12 axial force and shear force for all postures

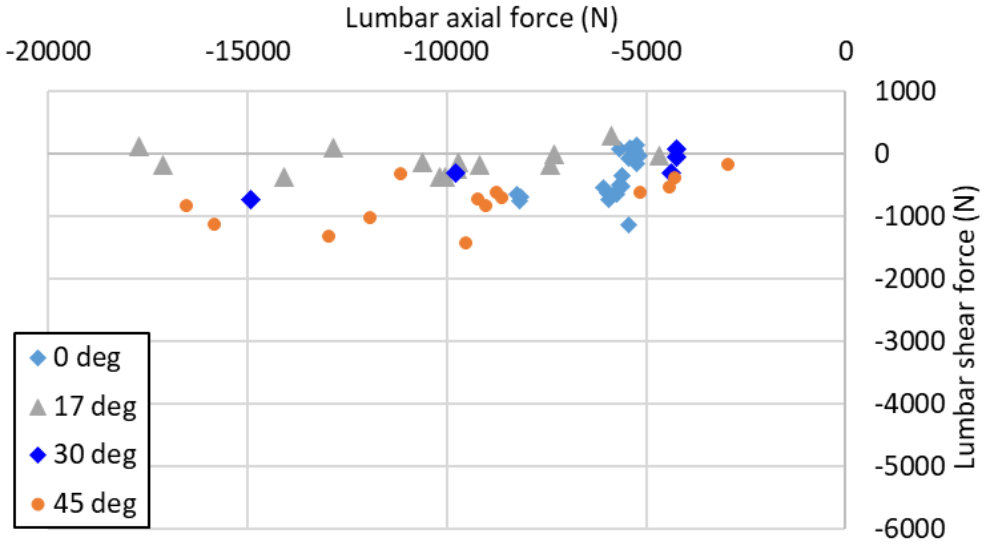

Figure 7. Cross plot of the lumbar axial force and shear force for all postures

At T12, the variation of peak axial and shear forces (time matched to the axial force peak) with velocity (Figure A-1, Appendix) for the reclined and nominal postures showed that all axial forces had R^2 values more than 0.9 while shear forces had R^2 values more than 0.9 with the exception for the 45° recline angle (0.6). All shear forces were along the antero-posterior axis for all postures, with a few exceptions for the 45° recline angle. At lumbar, the variation of peak axial and shear forces (time matched to the axial force peak) with velocity (Figure A-2, Appendix) for the reclined and nominal postures showed that all axial forces had R^2 values more than 0.9 while shear forces had R^2 values more than 0.8 for the 30° and 45°, and more than 0.6 for the 0°, and approximately 0.3 for the

30° recline angle. Shear forces were along the antero-posterior direction for all 45° reclined angle tests. At ischial, the variation of peak axial and shear forces (time matched to the axial force peak) with velocity (Figure A-3, Appendix) for the reclined and nominal postures showed that all axial forces had R^2 values more than 0.9 for all except the 30° recline angle (>0.8). Shear forces had R^2 values more than 0.8 for all postures.

4.4. ATD Variation of Peak Moments Based on Recline Angles

Table 9 shows the peak moments at T12 and lumbar locations based on recline angles including the nominal posture. The maximum moments occurred at T12 across all postures. Global maxima flexion and extension moments occurred in different postures. However, the ranges of velocities were not identical across all recline and nominal postures.

Table 9. Bending Moment (Nm) Data

	Velocity (m/s)	T12	Lumbar
Nominal Posture			
Min	2.5	–253.7	–127.1
Max	3.7	–86.8	–32.7
Mean	2.7	–181.5	–68.8
Standard Deviation	0.4	46.4	26.3
Recline Angle 17°			
Min	1.9	–332.0	–116.1
Max	7.4	98.9	53.4
Mean	4.3	–125.3	59.7
Standard Deviation	1.6	125.0	54.2
Recline Angle 30°			
Min	1.8	68.3	48.9
Max	5.6	157.4	104.2
Mean	3.0	109.1	81.0
Standard Deviation	1.7	35.3	22.2
Recline Angle 45°			
Min	1.7	90.8	–74.5
Max	7.4	407.4	234.1
Mean	4.3	207.4	94.5
Standard Deviation	1.8	87.0	81.0

A comparison of the sagittal bending moments at the T12 and lumbar locations versus impact velocity for different postures are shown in Figures 8 and 9. Moments were greater at the T12 than at the lumbar location regardless of posture. Furthermore, at

any specific velocity, moments decreased with increasing recline angle and this trend was clearer at the T12 than the lumbar location.

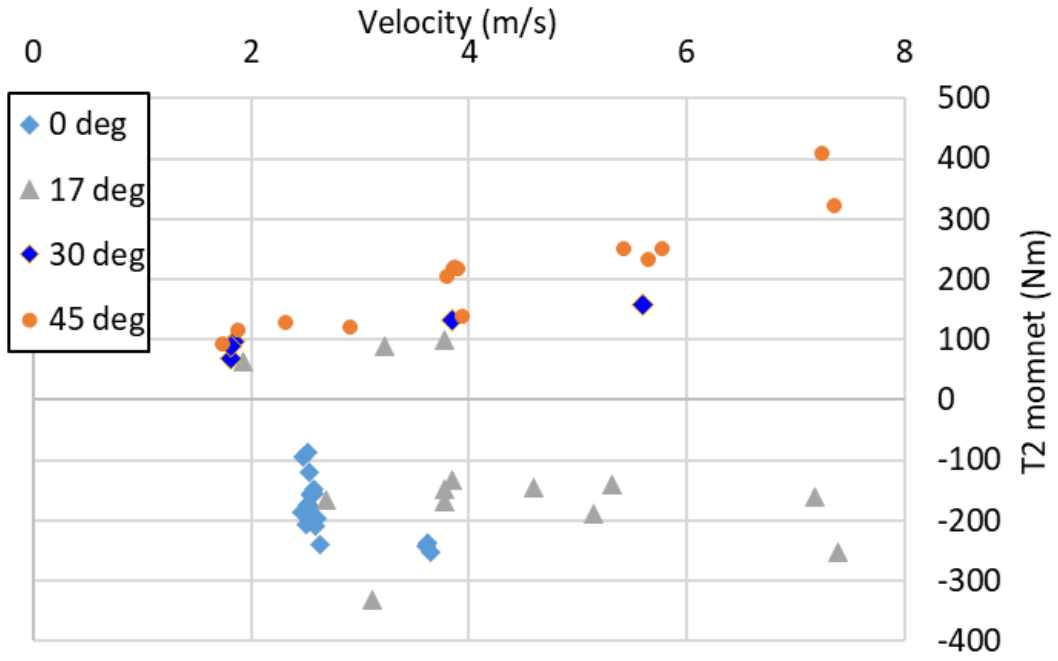

Figure 8. **Scatter plot of bending moments at T12 vs. velocity for all postures**

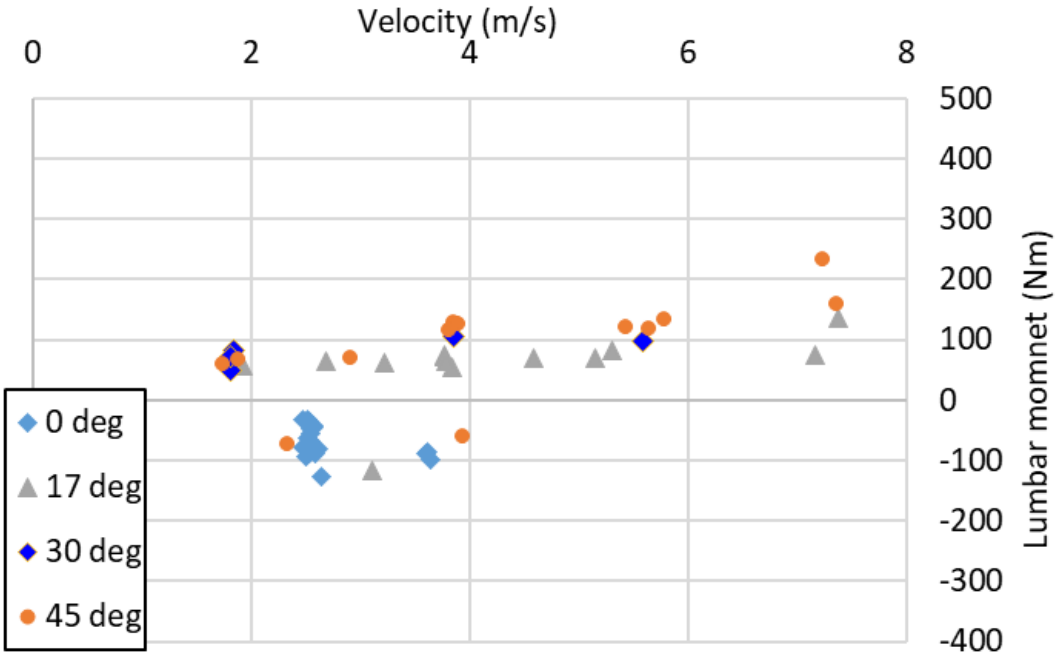

Figure 9. **Scatter plot of bending moments at lumbar vs. velocity for all postures**

4.5. PMHS Test Matrix and Summary of Forces

The mean age, height, weight and body mass index, and bone mineral density of the two male specimens were 61 ± 2.1 years, 167 ± 4.0 cm, 81 ± 26 kg, 29.1 ± 7.6 kg/m^2, and 186 ± 16.3 mg/cc, respectively. Table 10 shows the data for each specimen. The actual velocities were 8.8 and 10.0 m/s (mean 9.4 ± 0.9 m/s) for the two specimens, labelled as PV0200 and PV0201, respectively.

Table 10. Specimen Demographics

PMHS No.	Age (years)	Stature (cm)	Weight (kg)	Body Mass Index (kg/m^2)	Bone Mineral Density (mg/cc)
200	59	170	100	34.5	198
201	62	165	63	23.7	176
Mean	61	167	81	29.1	186
Std Dev	2.1	4.0	26	7.6	16.3

4.6. Biomechanical Data: Peak Loads, Accelerations, and Strains

Peak seat forces for the PV0200 and PV0201 specimens were 33.8 and 42.9 kN, respectively. Peak resultant sacrum, iliac, and pubis accelerations for these specimens were 322 and 396 g, 151 and 503 g, and 222 and 678 g, respectively. Table 11 shows the component-based data for these accelerations for each specimen. Peak spinal shear and axial forces and moments for the PV0200 specimen were 2446 N, 9294 N, and 327 Nm, respectively, and for the PV0201 specimen, these data were 2728 N, 11,650 N, and 503 Nm, respectively (Table 12). Tables 13 and 14 show the peak strain-gage recorded strains at different locations on the spine and pelvis. A separate document that includes the time histories of the axial, shear and resultant forces, and local accelerations and strains, and seat forces for both PMHS specimens is held by DAC and can be requested.

Table 11. Peak Sacrum, Iliac, and Pubis Accelerations for the Two Specimens

ID/Parameter		Peak Sacrum Acceleration (g)				Peak Iliac Acceleration (g)				Peak Pubis Acceleration (g)			
		x-axis	x-axis	z-axis	Res.	x-axis	x-axis	z-axis	Res.	x-axis	x-axis	z-axis	Res.
PV0200	Max	154	69	276	322	122	100	151	122	128	49	83	222
	Min	–120	–67	–318	. . .	–99	–126	. . .	–99	–113	–74	–209	. . .
PV0201	Max	302	180	264	396	77	218	503	77	438	219	146	678
	Min	–233	–133	–344	. . .	–304	–247	. . .	–304	–273	–651	–256	. . .

Table 12. Peak Axial, Shear, and Resultant Forces and Bending Moments for the Two Specimens

ID No.	Parameter	Spine Force (N) and Moment (Nm) peaks			
		Shear Force	Axial Force	Resultant Force	Moment
PV0200	Max	1810	793	9532	327.4
	Min	–2446	–9294	. . .	–0.1
PV0201	Max	2728	399	11753	503.2
	Min	–457	–11650	. . .	–52.4

Table 13. Peak Strains (μ) at Different Localized Regions of the Pelvis for the Two Specimens

ID No.	Parameter	Mid-Ilium		SI Joint		Posterior Ring		Ant Inf Iliac Spine	
		Right	Left	Right	Left	Right	Left	Right	Left
PV0200	Max	2370	1265	1080	254	407	333	490	1312
	Min	–404	–129	–155	–1153	–1389	–1523	–181	–79
PV0201	Max	1622	3063	3493	1055	1254	261	1803	120
	Min	–67	–363	–3775	–1659	–748	–4787	–1321	–1066

Table 14. Peak Strains (μ) at Different Localized Regions of the Ramus, Sacral Ala, and Spine for the Two Specimens

ID No.	Parameter	Superior Ramus		Inferior Ramus		Sacral Ala		L5 Vertebral Body
		Right	Left	Right	Left	Right	Left	
PV0200	Max	514	4180	720	1179	494	287	2017
	Min	–94	–261	–318	–590	–522	–376	–2499
PV0201	Max	459	7905	774	792	2759	2338	872
	Min	–567	–6	–1007	–1563	–345	–1954	–3007

4.7. Injuries

Injuries to PV0200 included fracture at the anterior inferior tip of the L4 vertebral body and sacral fractures (Figure 10). Both spine and sacrum injuries were considered clinically stable, and each injury was associated with AIS = 2 severity. Injuries to PV0201 included sacrococcygeal fractures with dislocation and facet fracture, bilateral diastasis of the sacroiliac joint, and anterior and posterior pubic rami fractures (Figure 11). The sacroiliac joint and pelvic injuries were considered unstable (AIS = 4, each) while the spine injury (AIS = 2) was considered stable. Table 15 lists the injuries and AIS-2015 codes for both specimens. A spine injury in PV0200 and an iliac wing fracture in PV0201 were not coded because they were considered as artifacts and are discussed in the next section.

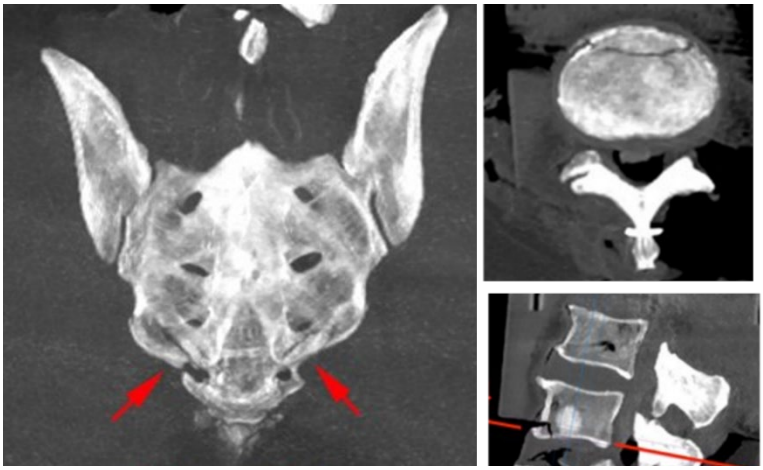

Figure 10. Injuries to the PV0200 specimen: sacral fractures (left, CT image, arrows show bilateral fractures), L4 anterior inferior body fracture (middle, top, axial CT image), L4 tip fracture (right, midsagittal CT image)

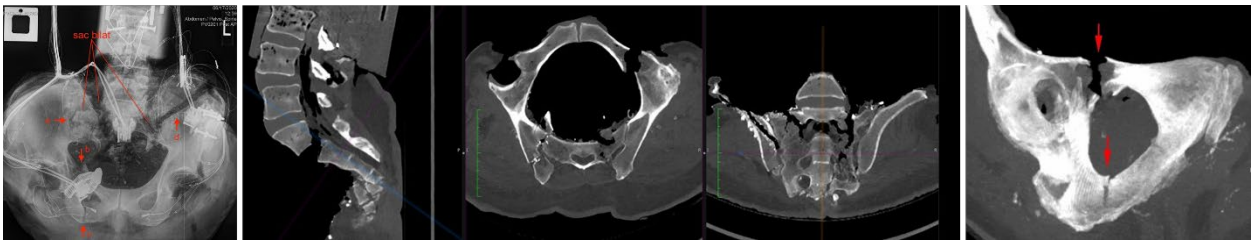

Figure 11. Injuries to the PV0201 specimen: pelvis (X-ray to the left), sacrococcygeal fractures with dislocation and facet fracture (sagittal CT image, second from left), bilateral SI diastasis (third and fourth CT scans from left), and anterior and posterior pubic rami fractures (axial CT scan, right)

Table 15. Injuries and AIS-2015 Description and Codes

ID No.	Injury Description	AIS-2015 Code
PV0200	L4 anterior inferior vertebral body fracture <20% compression	650632.2
	Distal sacral fracture	856151.2
PV0201	Complete disruption of posterior arch/SI diastasis unstable bilaterally Pubic rami fractures, anterior and posterior rami bilateral Sacral fracture-complete disruption, sacrococcygeal fracture with dislocation	856171.4
	L4 facet fracture	650422.2

In addition, complete dislocation of the spine at the mid-height of the L5 vertebra occurred for PV0200 and a fracture of the iliac wing was documented for PV0201. The reasons for not coding are discussed in the next section.

5. DISCUSSION

5.1. ATD Discussion of Results

The purpose of conducting tests in postures other than the nominal posture was to examine the feasibility of the ATD to align along different reclined positions and sense the transmitted loads at the ischial, lumbar, and T12 locations. The selection of the recline angles, defined using the lumbar spine orientation, was based on the expectations of possible ranges in occupant variations and future seat designs in military vehicles, while acknowledging that all possible future seat and seat structure designs are not known. The overall goal of the use of the off-nominal posture data was to examine whether the current IARCs developed for the nominal posture are applicable to other recline angle or angles, and the present analysis is a first step.

To achieve these goals, the present series of analysis was done for the group of 53 tests (20 nominal, 5 at 30° recline, and 14 each in the 17° and 45° recline angles) that were not reported in earlier reports submitted to the WIAMan program. The velocities were somewhat uniform (approximately same range) for all tests except the nominal posture in which they spanned a short and lower-end range. The following discussion applies to this test matrix, and the authors expect that the conclusions drawn in this report are applicable across all tests to the velocity ranges used in reclined postures. The current analysis from previously conducted tests is a component of a larger ongoing analysis by the sponsor. The peak axial and shear forces developed in the reclined tests fall within the range of those forces when data were compared at similar velocities. This is to be expected because the ATD is infrangible under all magnitudes of velocities, while shear factors vary due to recline angulations. Like forces, based on the peak magnitudes of sagittal bending moments, the load cell capacities appear to be adequate for all reclined postures considered in this study.

The ratio of the time-matched shear force to the peak axial force, that is, the F_x/F_z shear factor, was used as a candidate parameter to determine the effectiveness of the IARCs. The selection had the following rationale. In the nominal posture, the expectation is that the axial forces dominate with minimal contribution from shear forces. This is because the loading is vertical, the surrogate is aligned in a seated-Soldier/vertical posture, and sagittal bending of the spine is minimal. Injuries documented in earlier PMHS tests offer support to this concept as they were primarily axial compressive-force-induced fractures to the lumbar spine in isolated lumbar spine tests, and similar fractures in subsystem pelvis–lumbar spine vertical loading tests.[1,7] In both biological models, the specimens were aligned according to the seated-Soldier posture.[2] The shear factor was obtained at the time of the peak axial force and not calculated as the ratio of the peak shear force to the peak axial force. This is because both force components develop simultaneously

albeit with different rates, peak axial force precedes the development of the peak shear force, and injuries in the nominal posture from previous PMHS tests were associated with the axial compressive rather than the shear or bending mechanism in addition to the compressive component.

In contrast to the axial force dominance associated with the nominal posture, increasing recline angulations should involve increasing contributions from the shear component, that is, greater bending of the pelvis–lumbar spine complex. The contribution of the shear is expected to be the greatest at the T12 location due to the length of the spinal column and its distal location from the impact site, that is, pelvis, while the contribution at the lumbar and ischial ends should be minimal due to their proximities to the impact site. As presented in Table 8, at T12 the shear factor decreased from the nominal to the recline 17°, 30°, and 45° posture tests (mean values of 0.5 for the nominal to 0.3 to 0.1 to 0.1 for the three recline angles, respectively). An explanation to the unexpected trend is as follows.

In the nominal posture, the pelvis flesh is fully in contact with the plate, the initiation of impact loading compresses the flesh, induces axial loading to the proximal regions of the pelvis (compressive forces at the ischial and lumbar load cell), and deforms the lumbar column. At the interface of the spine material with the rigid load cell at T12, deformation/relative motion of the spine along the antero-posterior axis produces a shear force in the T12 load cell. The mismatch in the rigidity of the load cell and the deformability of the rubber spine material induces the shear, while the entire pelvis–lumbar spine assembly is constrained by the seat platen and the upper-carriage ballast mass, and these double end-constraint conditions occur during the loading phase. In other words, the peak axial force develops during the loading event while both end constraints are active (seat platen has not started to decelerate) and the shear is of considerable magnitude. This phenomenon is consistent across all velocities because the ATD is infrangible, while the same may not apply for PMHS because higher velocities tend to injure the specimen, limiting the development of the shear force. At the lumbar location, the magnitudes of the shear factor were lower (than T12): 0.07, 0.02, and 0.04 for the nominal, reclined 17° and 30° postures, respectively; however, it was somewhat greater for the 45° posture (0.07 for T12 and 0.09 for lumbar). This is to be expected because of the proximity of the load cell to the impact location. A similar expected pattern was present at the ischial location, despite the low magnitudes of the forces contributing to the normalizing process. Because the current IARCs do not use the ischial axial or shear force as an injury metric, this issue may be of secondary significance.

In the reclined posture, an explanation for the forces and moments associated is as follows. While the initiation of impact loading still compresses the pelvis flesh, the compression is less uniform compared to the nominal posture. This is because the reclined angulation decreases the contact surface area. Increased reclined angulations allow greater rotation of the inferior end of the pelvis-spine subsystem, thereby decreasing the constraint compared to the nominal posture imposed at the pelvic end. The decreased constraint reduced the development of the shear force, shear factor, and the bending moment and this phenomenon increased with increased recline angles.

This data analysis was based on the temporal development of axial and shear forces at different locations on the WIAMan ATD. The current IARCs use the resultant force as a metric. The analysis replacing the axial force with resultant force to determine the shear factor produced lower magnitudes for each case: posture and location. Because this method uses the resultant force as the normalizing variable, the ratios are lower than those from the previous method and a comparison between the two methods are shown in Figure 12. Because the two methods result in almost the same magnitudes of the shear factor, earlier discussions on the role of the shear factor are applicable to the resultant force-based analysis of reclined posture tests analyzed in this study.

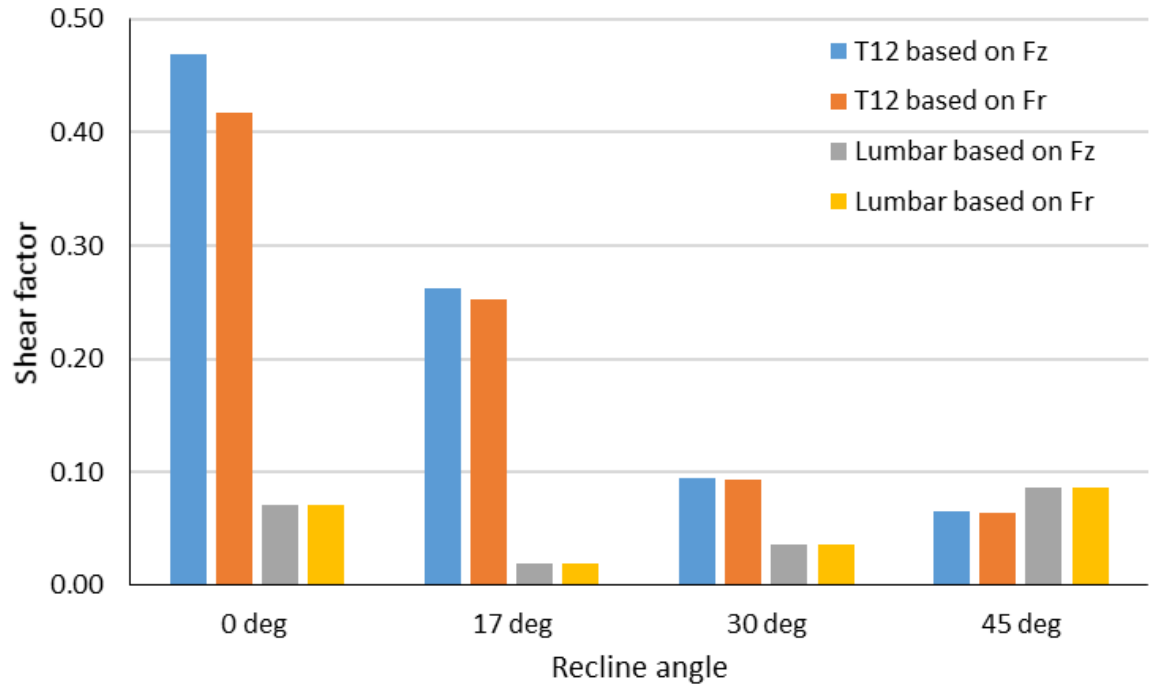

Figure 12. The mean shear factors at T12 and lumbar using the axial and resultant forces

5.2. PMHS Discussion of Results

The purpose of conducting PMHS tests in postures other than the nominal posture was to determine injuries, injury mechanisms, and spinal loads, and compare them to nominal posture data with the long-term goal of investigating whether the human injury probability curves (HIPCs) and IARCs (from WIAMan ATD tests) differ between postures. While the superior end of the spine was angulated by 45° in both specimens, the orientation of the pelvis was based on the anatomy of specimen. Because the pelvis recline angles were approximately the same in both specimens, 58° and 61°, it is possible to compare biomechanical data from the two specimens with the acknowledgment that statistical analysis is not meaningful from two biological specimen outputs, and hence, a descriptive analysis is presented as a first step. An examination of the peak forces between the two tests showed similar magnitudes when normalized to either velocity input. Upon normalization to the common average velocity of 9.4 m/s, the resultant forces (10.2 vs. 11.0 kN) differed by less than 8%, and the axial forces (10.0 and 9.9 kN) differed by less than 1%. This is considered within the biological variability of the PMHS. From this perspective, the two experiments conducted with similar test parameters of the vertical accelerator device (Table 3) produced similar levels of impact to both specimens. Because the axial force is the major driving insult, injuries are expected to be similar, except for biological variations, deemed minimal from normalized peak force analysis. In other words, compression-related injuries should occur of similar severity to the pelvis and or the spine.

In the PV0200 test, an examination of the high-speed video images indicated that, upon the initiation of impact, the pelvis of the specimen absorbed the initial impact, and continued to load the pelvis–spine complex, essentially compressing the sacroiliac and spinal joint and the surrounding bony complexes. The stable fracture of the distal sacrum and anterior inferior tip of the L4 vertebral body were attributed to compressive forces from vertical impact. These types of injuries were observed in nominal postural tests in the previous WIAMan test series.[1,5,8] Upon unloading of the specimen, the seat plate began to retract while the pelvis–lumbar continued its vertical travel, and at the end of the experiment, the carriage came to a stop at the top of the vertical accelerator tower, completely disarticulating the specimen distally and components superior to the mid-L5 level were hanging loose. This unexpected injury in the form of a mid-body-posterior complex fracture with complete dislocation of the entire specimen at the L5 vertebra level was, therefore, considered an experimental artifact. The fracture path traversed the middle of the entire vertebra (Figure 13). The total dislocation injury at the mid-body level did not involve the superior and inferior intervertebral discs. Such complete disarticulation of the lower lumbar spine at the mid-body-posterior complex is not reported in civilian and military clinical literatures. To the best knowledge of the

academic and government authors of this analysis, they do not occur under in-vivo situations from under-body blast loading events because of the presence of the torso restraint (five-point harness) worn by Warfighters. For the same reasons, such injuries are also not expected in reclined postures.

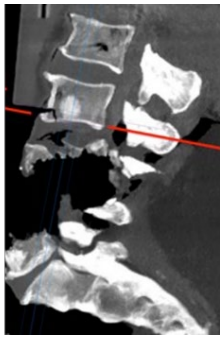

Figure 13. CT image showing the transection of the spine at mid-vertebra level. This is considered an experimental artifact.

To prevent the transection of the specimen that occurred at the end of the experiment for PV0200, modifications were made during the preparation of the PV0201 specimen. The pelvis–spine complex was contained in a netting and fixed to the superior fixation before impact loading. This proved successful. After the impact event, an examination of the high-speed video images indicated similar kinematics as the PV0200 specimen, with the previous exception of no transection/artifactual injury at the end the experiment. Injuries included sacrococcygeal fractures with dislocation and facet fracture, bilateral diastasis of the sacroiliac joint, and anterior and posterior pubic rami fractures. The sacroiliac joint and pelvic injuries were considered unstable (AIS = 4, each) and spine injury (AIS = 2) was considered stable. These injuries were directly attributed to the impact loading and consistent with the greater load sustained by the pelvis (25% greater energy input) in the PV0201 than the PV0200 specimen. The early attainment of the strains approximately in line with the peak seat forces, sacrum, or iliac accelerations, are internally consistent.

In this PV0201 specimen, the fracture of the left iliac wing was attributed to the artifact of the contact of the metallic mount attached to the superior end with the left side of the pelvis. The fracture likely occurred after the right-sided fractures of the pelvis. The right side of the pelvis sustained compression as shown by the inferior ramus strain profiles: right side responding with compressive strain early in the loading phase, and with continued loading, left ramus sustained compression later. As the specimen sustained the impact from the seat, the pelvis began to compress and the initiation of the angulation of the pelvis with respect to the spine (flexed pelvis) induced injuries to the right side, allowing the left side of the iliac wing to contact the rigid edge of the metallic fixture and inducing a local fracture to the wing. The image shown in Figure 14 aligns

the X-ray fracture line with the metal edge (drawn for clarity). Severe injuries sustained by the inferior regions of the pelvis–lumbar complex, that is, pelvis and sacrum, likely spared the spine from sustaining severe injuries. This is expected as fracture and energy absorption are related. This analysis is limited to one specimen where the end condition may have altered the load path within the pelvis, resulting in an unexpected left iliac wing fracture. The asymmetry of the pelvis–spine anatomy of the specimen may have also contributed to the unilateral injuries. Additional tests are needed to confirm the absence of this artifactual fracture after modifying the metallic fixture. Tests with the whole lumbar spinal column may avoid/minimize this end-condition effect.

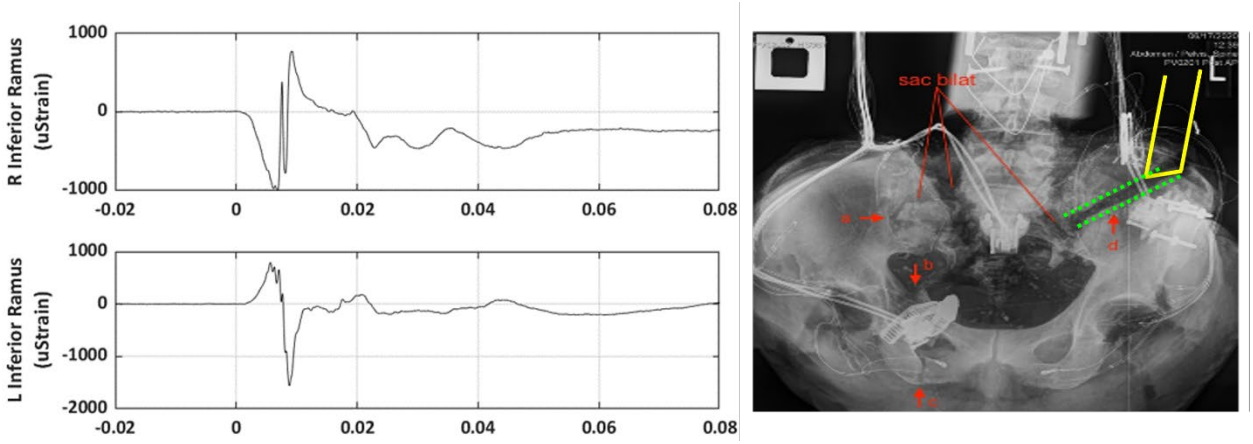

Figure 14. Time history plots show the strains on the right (top) and left (bottom) ramus. Note the negative (compressive) strain profile on the right side while the positive strain precedes the negative strain on the left ramus. The iliac wing fracture is shown on the X-ray, with the dotted lines encompassing the fracture. The yellow lines show the approximate profile of the metallic edge of the fixation that contacted the pelvis resulting in the local depression and fracture of the left wing.

5.3. Summary of ATD and PMHS Findings

Data were analyzed from 53 tests from vertical loading to the WIAMan ATD-isolated pelvis–lumbar spine aligned in different postures. Peak forces and moments were greater at the T12 than at the lumbar location for all postures. Reclined postures showed differing proportions of the axial and shear forces at the T12 and lumbar locations on the spine. Using this as a basis, the shear factor metric was defined to include the temporal development of both force components, addressing the potential injury mechanisms. The shear factors at the T12 location were 0.5 for the nominal, 0.3 for the 17° recline, 0.1 for the 30° recline and 0.1 for the 45° postures. The same trend in the shear factor was obtained when the axial force was replaced by the resultant force, although the magnitudes were lower in all cases. The shear factors were lower for the lumbar location in both cases.

Data were analyzed from two PMHS tests, injuries were identified, and forces and moments at the spinal end were obtained. Both specimens produced injuries to the pelvis and spine, while some artifactual injuries occurred. Types of injuries and severities as scored using the AIS-2015 version were similar to those previously conducted nominal posture tests under the WIAMan Program.[1,5,8–11] The samples' sizes were too limited to draw statistical conclusions, including the development of HIPCs. These findings are applicable to the analysis of previously conducted WIAMan ATD tests. Analysis from other tests in the WIAMan database can be included to reinforce the present findings, and experiments with PMHS in different recline postures are needed to confirm the role of the shear/bending of the spine on injuries and injury mechanisms.

6. CONCLUSION AND RECOMMENDATIONS

The experimental design and protocols used in the study showed the feasibility of conducting ATD and PMHS tests in reclined postures. The tested version of the WIAMan ATD appears to be suitable to evaluate the performance in under-body blast loadings under different postures: nominal to recline, potentially reflecting future seat and vehicle designs in the military. The biomechanical responses analyzed from the PMHS data showed that injuries parallel nominal postures and spinal loads can be determined, and mechanical responses from the ATD data demonstrated that component-based contributions of axial and shear forces and bending moments depend on the postural angulation. Analysis of these previous tests, with limited PMHS data supporting ATD findings, has laid a foundation to conduct additional experiments as this is the first step to develop IARCs with ATD matched-pair tests. In this analysis study, the shear factor was used as a biomechanical metric for quantifying the responses of the pelvis–lumbar spine of the Gen-1 ATD because it accommodated both the axial and shear forces in the time domain. The recognition that the shear factor did not significantly change with different reclined postures considered in this series of tests, the current IARCs developed for only the nominal posture, may also be applicable to reclined postures with this ATD. As reclined postures may be common in future seat designs, and as the WIAMan ATD has already shown its feasibility to be aligned with different postural conditions, the current set of limited PMHS and ATD tests provides confidence in additional matched-pair studies. Once injuries, injury mechanisms, and HIPCs from PMHS and IARCs from WIAMan ATD are developed, it is possible to fully quantitate the efficacy of current IARCs-based nominal posture to reclined postures.

7. REFERENCES

1. Yoganandan, N., Moore, J., Humm, J. R., Baisden, J. L., Banerjee, A., Pintar, F. A., Barnes, D. R., & Loftis, K. L. (2021). Human pelvis injury risk curves from underbody blast impact. *BMJ Mil. Health*. doi:10.1136/bmjmilitary-2021-001863 [published online first: 2021 October 30]

2. Reed, M. P., & Ebert, S. M. (2013, October 31). The seated Soldier study: posture and body shape in vehicle seats. Retrieved February 2022, from https://pdfs.semanticscholar.org/f4f8/ad73a06bcebd6c97c2deff01dcdd57f5b2fb.pdf.

3. Rupp, J. M. C., Bonifas, A., Ott, K., Demetropoulos, C., Gipple, J., Sherman, D., Cavanaugh, J., Barnes, D., & Loftis, K. (2021, April). *Warrior injury assessment manikin (WIAMan) generation 1 anthropomorphic test device (ATD) positioning in highly reclined and other alternative postures* (Report No. DEVCOM-DAC-TR-2021-021). DEVCOM Analysis Center.

4. Yoganandan, N., Pintar, F. A., Schlick, M., Humm, J. R., Voo, L., Merkle, A., & Kleinberger, M. (2015). Vertical accelerator device to apply loads simulating blast environments in the military to human surrogates. *J. Biomech.*, *48*(12), 3534–8. doi:10.1016/j.jbiomech.2015.06.008 [published online first: 2015, July 15]

5. Salzar, R. S., Spratley, E. M., Henderson, K. A., Greenhalgh, P. C., Zhang, J. Z., Perry, B. J., & McMahon, J. A. (2020). The mechanical response and tolerance of the anteriorly-tilted human pelvis under vertical loading. *Annals of Biomedical Engineering*. doi:10.1007/s10439-020-02634-6 [published online first: 2020, September 26]

6. Association for the Advancement of Automotive Medicine. (2015). *Abbreviated injury scale: 2015 revision* (6 ed.).

7. Yoganandan, N., Moore, J., DeVogel, N., Pintar, F., Banerjee, A., Baisden, J., Zhang, J. Y., Loftis, K. L., & Barnes, D. (2020). Human lumbar spinal column injury criteria from vertical loading at the base: Applications to military environments. *J. Mech Behav Biomed Mater.*, *105*, 103690. doi:10.1016/j.jmbbm.2020.103690 [published online first: 2020, April 14]

8. Yoganandan, N., Moore, J., Humm, J. R., Baisden, J. L., Pintar, F. A., Barnes, D. R., & Loftis, K. L. (in press). Loading rate effects on trade-off of fractures from pelvis to lumbar spine under axial impact loading. *Traffic Inj Prev*.

9. Danelson, K., Watkins, L., Hendricks, J., Frounfelker, P., Team WICR, Pizzolato-Heine, K., Valentine, R., & Loftis, K. (2018). Analysis of the frequency and mechanism of injury to warfighters in the under-body blast environment. *Stapp Car Crash J.*, *62*, 489–513. [published online first: 2019, January 05]

10. Danelson, K. A., Kemper, A. R., Mason, M. J., Tegtmeyer, M., Swiatkowski, S. A., Bolte, J., & Hardy, W. N. (2015, November 9). Comparison of ATD to PMHS response in the under-body blast environment. *Stapp Car Crash J.*, *59*, 445–520. [published online first: 2015, December 15]

11. Barnes, D. R., Yoganandan, N., Moore, J., Humm, J., Pintar, F., & Loftis, K. L. (2021). Quantifying the effect of pelvis fracture on lumbar spine compression during high-rate vertical loading. *Stapp Car Crash J.*, *65*, 189–216. doi:10.4271/2021-22-0008 [published online first: 2022, May 06]

Appendix A – Test Matrix and Regression Plots

Table A-1. Test Matrix

Test ID	Recline Angle (deg)	Velocity (m/s)	TTP (ms)	Test ID	Recline Angle (deg)	Velocity (m/s)	TTP (ms)	Test ID	Recline Angle (deg)	Velocity (m/s)	TTP (ms)
PG1D200	0	2.4	13	PG1D218	0	4	5	PG1D236	45	4	10
PG1D201	0	2.4	13	PG1D219	0	4	5	PG1D237	45	3	5
PG1D202	0	2.4	13	PG1D220	17	2	10	PG1D238	45	3	15
PG1D203	0	2.4	13	PG1D221	17	4	10	PG1D239	45	5	5
PG1D204	0	2.4	13	PG1D222	17	6	10	PG1D240	45	5	15
PG1D205	0	2.4	13	PG1D223	17	4	10	PG1D241	45	3	5
PG1D206	0	2.4	13	PG1D224	30	2	10	PG1D242	45	4	10
PG1D207	0	2.4	13	PG1D225	30	2	10	PG1D243	17	4	10
PG1D208	0	2.4	13	PG1D226	30	4	10	PG1D244	17	3	5
PG1D209	0	2.4	13	PG1D227	30	6	10	PG1D245	17	3	15
PG1D210	0	2.4	13	PG1D228	30	2	10	PG1D246	17	5	5
PG1D211	0	2.4	13	PG1D229	45	2	10	PG1D247	17	5	15
PG1D212	0	2.4	13	PG1D230	45	4	10	PG1D248	17	4	10
PG1D213	0	2.4	13	PG1D231	45	6	10	PG1D249	17	3	15
PG1D214	0	2.4	13	PG1D232	45	4	10	PG1D250	17	7	5
PG1D215	0	2.4	13	PG1D233	45	4	10	PG1D251	17	7	15
PG1D216	0	2.4	13	PG1D234	45	7	5	PG1D252	17	4	10
PG1D217	0	4	5	PG1D235	45	7	15	. . .	. . .	. . .	. . .

Note: TTP = time-to-peak

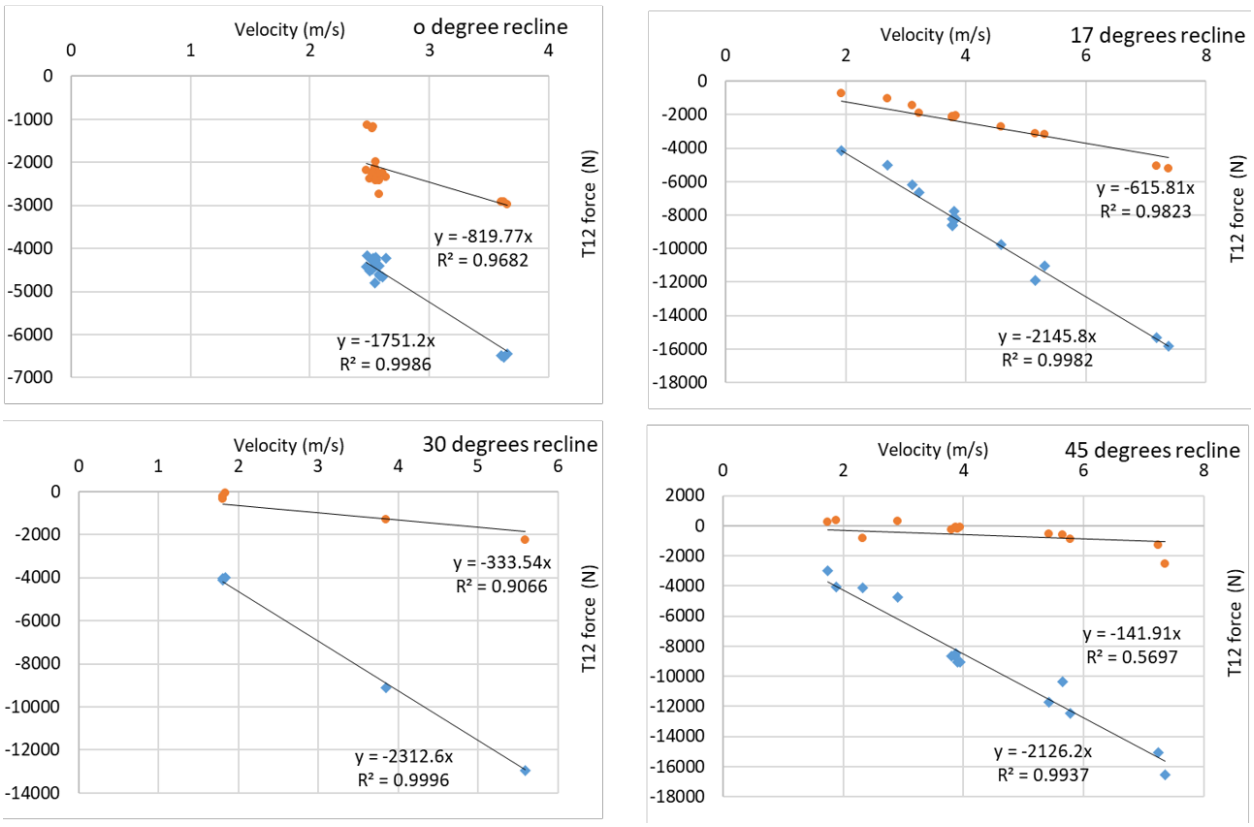

Figure A-1. Linear regression relationships of the axial and shear forces at T12 for all postures. Axial forces are shown in diamonds and shear forces are shown in circles, and recline angulations are indicated at top right.

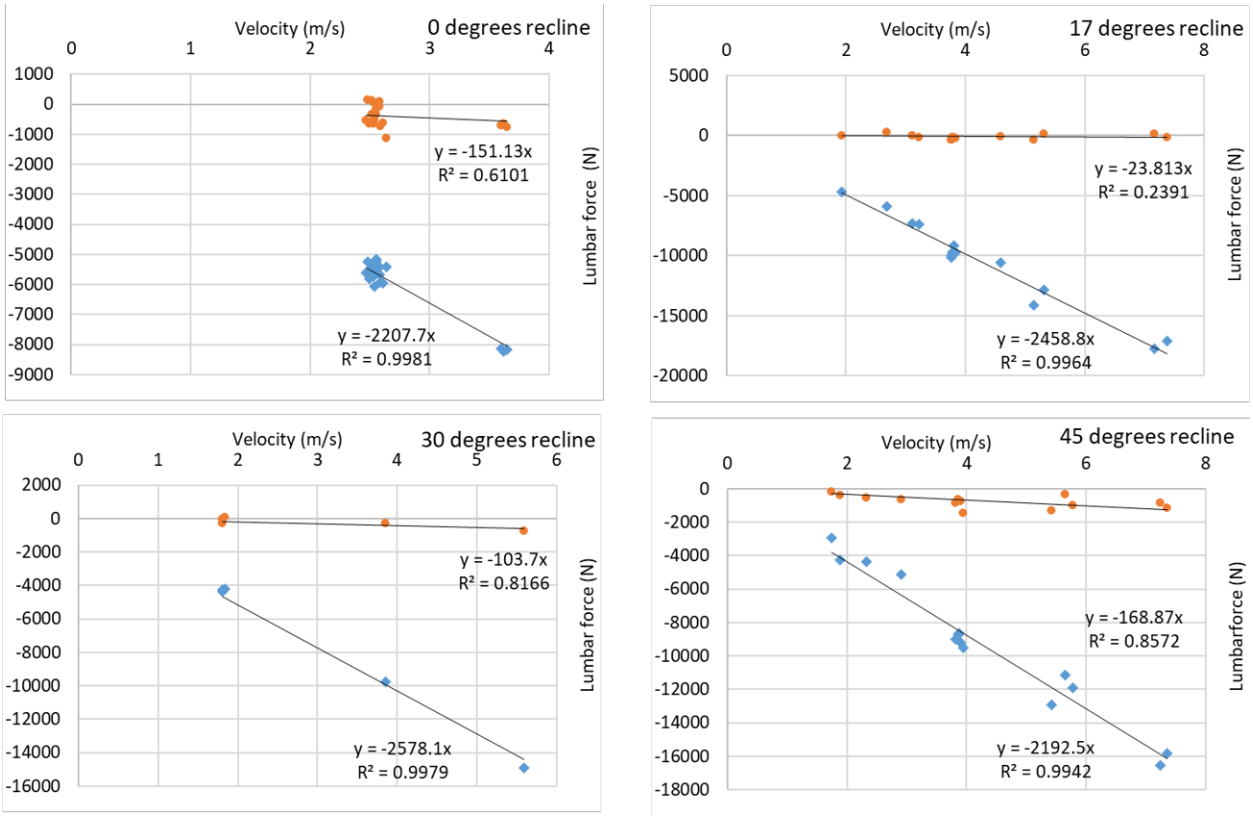

Figure A-2. Linear regression relationships of the axial and shear forces at lumbar for all postures. Axial forces are shown in diamonds and shear forces are shown in circles, and recline angulations are indicated at top right.

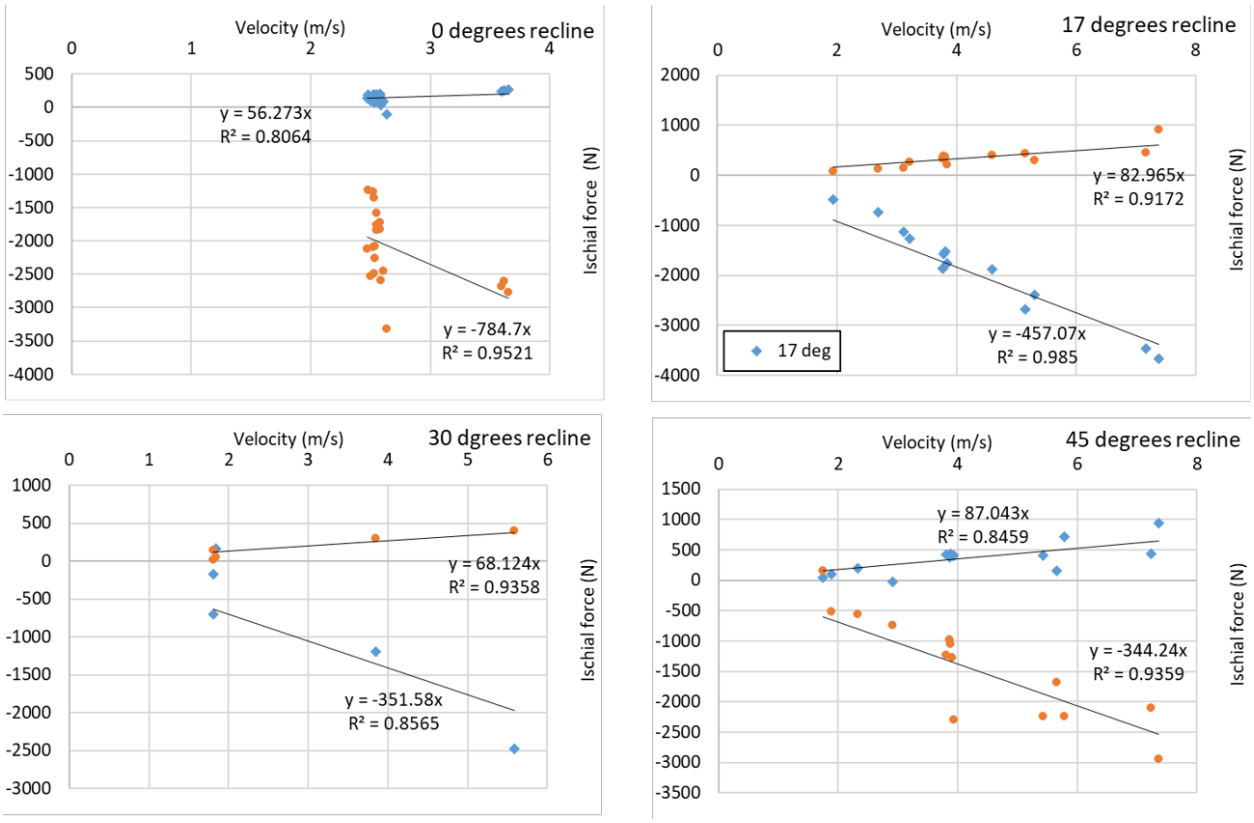

Figure A-3. Linear regression relationships of the axial and shear forces at ischial for all postures. Axial forces are shown in diamonds and shear forces are shown in circles, and recline angulations are indicated at top right.

LIST OF ACRONYMS

AIS	Abbreviated Injury Scale
ATD	anthropomorphic test device
CT	computed tomography
DAC	DEVCOM Analysis Center
DEVCOM	U.S. Army Combat Capabilities Development Command
Gen	Generation
HIPC	human injury probability curve
IARCs	injury assessment reference curves
ID	identification
MCW	Medical College of Wisconsin
PMHS	postmortem human surrogate
SI	sacroiliac
TTP	time-to-peak
WIAMan	Warrior Injury Assessment Manikin: Army-sponsored program to develop an ATD specifically designed to predict injury risk in vertical loading environments

ORGANIZATION

U.S. Army DEVCOM Analysis Center
FCDD-DAD-TP/G. Dietrich
FCDD-DAG-S/K. Loftis
FCDD-DAG-S/K. Sandora
FCDD-DAG-S/G. Steiger
FCDD-DAG-S/B. Vanamburg
6896 Mauchly St.
Aberdeen Proving Ground, MD 21005-5071

U.S. Army Evaluation Center
Survivability Evaluation Directorate
TEEC-SV/R.J. Spink
6617 Aberdeen Blvd., Bldg 2202, 2nd Floor
Aberdeen Proving Ground, MD 21005-5071

U.S. Army DEVCOM Ground Vehicle Systems Center
FCDD-GVR-VMT/D. Weyland
FCDD-GVR-VMT/R. Scherer
6501 E. 11 Mile Rd
Detroit Arsenal, MI 48397-5000

Office of the Director, Operational Test and Evaluation
OSD DOT&E
LFT&E/J. Ivancik
1700 Defense Pentagon 1D548
Washington DC 20301

Medical College of Wisconsin
N. Yoganandan
J. Moore
J. Humm
J. Baisden
F. A. Pintar
8701 Watertown Plank Road
Milwaukee, WI 53226

DEVCOM Army Research Laboratory
FCDD-RLD-DCI/Tech Library
2800 Powder Mill Rd.
Adelphi, MD 20783

Defense Technical Information Center
ATTN: DTIC-O
8725 John J. Kingman Rd.
Fort Belvoir, VA 22060-6218